Fast Solution of Electromagnetic Integral Equations Using Adaptive Wavelet Packet Transform

Hai Deng, *Student Member, IEEE,* and Hao Ling, *Fellow, IEEE*

***Abstract*—The adaptive wavelet packet transform is applied to sparsify moment matrices for the fast solution of electromagnetic integral equations. In the algorithm, a cost function is employed to adaptively select the optimal wavelet packet expansion/testing functions to achieve the maximum sparsity possible in the resulting transformed system. The search for the best wavelet packet basis and the moment matrix transformation are implemented by the repeated two-channel filtering of the original moment matrix with a pair of quadrature filters. It is found that the sparsified matrix has above-threshold elements that grow only as $O(N^{1.4})$ for typical scatterers. Consequently the operations to solve the transformed moment equation using the conjugate gradient method scales as $O(N^{1.4})$. The additional computational cost for carrying out the adaptive wavelet packet transform is evaluated and discussed.**

***Index Terms*—Electromagnetic scattering, fast solution methods, wavelet transform.**

I. Introduction

In solving electromagnetic integral equations, the application of the method of moments procedure with conventional expansion and testing functions always results in a dense moment matrix. For a problem of size N, the direct solution of the moment equations requires $O(N^3)$ operations, which is prohibitively expensive for large-scale scattering problems. Recently there has been much interest in using wavelet basis to sparsify the dense moment matrix, leading to reduced solution time for the resulting sparse matrix equation [1]–[8]. It has been found that the application of wavelet basis functions in electrodynamic problems can result in a very sparse moment matrix after a thresholding operation. Unfortunately, the number of nonzero elements still grows on the order of $O(N^2)$ when the problem size is increased [5]. As a result, the computational complexity of solving electromagnetic integral equations using the wavelet basis transform is not reduced significantly.

The above drawback of the conventional wavelet transform (CWT) method for electrodynamic problems has been explained by us earlier in terms of the oscillatory nature of the electrodynamic kernel [7], [8]. The CWT implemented with multiresolution analysis is essentially a constant-Q decomposition of the signal in the frequency domain. (In this paper, the term frequency refers to spectral frequency since our signal space is defined in the spatial dimension.) For the signals with energy content centered around zero frequency, CWT can achieve a very efficient compression [9]. For electrodynamic problems, however, the Green's function is oscillatory around the spectral frequency k_0. Hence the more efficient way to compress the Green's function is to employ modulated bases which can zoom in on the center frequency k_0 automatically.

In this work, we apply the recently introduced adaptive wavelet packet transform (AWPT) [8], [10]–[12] to the sparsification of moment matrix. In this approach, the transformation bases in the AWPT are adaptively selected based on a cost function such that the transformed moment matrix has the maximum sparsity. Consequently, the AWPT transformed matrix is more efficiently represented than that using the CWT, as we abandon the rigid constant-Q decomposition structure of the CWT. We find that the resulting sparsified moment matrix from the AWPT can have nonzero grow only as $O(N^{1.4})$ for a number of test structures. Independent work on using wavelet packet basis for electromagnetic computation has been reported by Golik [13], [14], who generated a wavelet packet basis by decomposing the excitation vector.

This paper is organized as follows. In Section II, we first give a brief introduction of the moment equation transform with wavelet packet basis. We then introduce the search algorithm for the best wavelet packet basis and the implementation of the AWPT with repeated filtering of input data by a pair of quadrature filters. In Section III, we present numerical results of the moment matrix sparsification with the AWPT for several two-dimensional (2-D) scatterers. The results obtained with the CWT are also given for comparison. Finally the computation time of the AWPT procedure and the solution time for the sparsified system using an iterative conjugate gradient solver are provided. The conclusions are given in Section IV.

II. Moment Matrix Sparsification Using AWPT

Let us consider a moment matrix equation

$$[\boldsymbol{Z}]\boldsymbol{J} = \boldsymbol{E} \tag{1}$$

where $[\boldsymbol{Z}]$, $\boldsymbol{J}$, and $\boldsymbol{E}$ denote the moment matrix, the induced current vector, and the excitation vector, respectively. If the moment matrix $[\boldsymbol{Z}]$ is transformed with two orthonormal matrices $[\boldsymbol{M}_1]$ and $[\boldsymbol{M}_2]$, the equation can be changed into

$$[\boldsymbol{M}_2]^T[Z][\boldsymbol{M}_1][\boldsymbol{M}_1]^T\boldsymbol{J} = [\boldsymbol{M}_2]^T\boldsymbol{E} \tag{2}$$

Manuscript received September 9, 1997; revised November 20, 1998. This work was sponsored by the Joint Services Electronics Program under Contract AFOSR F49620-95-C-0045 and in part by the Air Force MURI Center for Computational Electromagnetics under Contract AFOSR F49620-96-1-0025.

The authors are with the Department of Electrical and Computer Engineering, The University of Texas at Austin, Austin, TX 78712-1084 USA.

Publisher Item Identifier S 0018-926X(99)04774-2.

or

$$[\tilde{\boldsymbol{Z}}]\tilde{\boldsymbol{J}} = \tilde{\boldsymbol{E}} \tag{3}$$

where

$$[\tilde{\boldsymbol{Z}}] = [\boldsymbol{M}_2]^T[\boldsymbol{Z}][\boldsymbol{M}_1] \tag{4}$$

$$\tilde{\boldsymbol{J}} = [\boldsymbol{M}_1]^T\boldsymbol{J} \tag{5}$$

and

$$\tilde{\boldsymbol{E}} = [\boldsymbol{M}_2]^T\boldsymbol{E}. \tag{6}$$

The transformation matrices $[\boldsymbol{M}_1]$ and $[\boldsymbol{M}_2]$ change the original expansion/testing functions into a new set of expansion/testing functions. Note that $[\boldsymbol{M}_1]$ and $[\boldsymbol{M}_2]$ are in general different, since the expansion and testing functions can be different. The objective is to find the best expansion/testing functions (therefore the two matrices $[\boldsymbol{M}_1]$ and $[\boldsymbol{M}_2]$) such that the transformed matrix $[\tilde{\boldsymbol{Z}}]$ has the maximum sparsity possible. Such a best basis for a given moment matrix $[\boldsymbol{Z}]$ will be selected from all possible wavelet packet bases. Once the transformation is completed, the resulting sparse system can be solved using an iterative solver to take advantage of the sparsity. The original induced current can be obtained from the solution of the transformed induced current $\tilde{\boldsymbol{J}}$ via

$$\boldsymbol{J} = [\boldsymbol{M}_1]\tilde{\boldsymbol{J}}. \tag{7}$$

In the following sections, we shall first introduce the wavelet packet concept and show that it can be considered as a generalization of the conventional wavelet basis. Next we outline the implementation of the moment matrix transformation using wavelet packet basis. Finally, we describe the search procedure for the best wavelet packet basis to arrive at a system with maximum sparsity.

A. Wavelet Packet Basis

Wavelet packet basis is a generalization of the commonly used wavelet basis [15]–[17]. It has all the major features of the conventional wavelet basis and can be defined from basic wavelet concepts. Let $\phi(\boldsymbol{x})$ and $\psi(x)$ be the scaling function and the corresponding wavelet mother function in the conventional wavelet transform and define $\psi_0(x) = \phi(x)$, and $\psi_1(x) = \psi(x)$. Using the well-known "two-scale equations," we can construct the wavelet packet basis in the $L^2(\Re)$ signal space as [15]–[17]

$$\begin{aligned}\psi_{2l}(x) &= \sum_k h(k)\psi_l(2x-k)\\ \psi_{2l+1}(x) &= \sum_k g(k)\psi_l(2x-k) \qquad l = 0,1,2\cdots\end{aligned} \tag{8}$$

where $\{h(k)\}$ and $\{g(k)\}$ are the impulse responses of two quadrature filters, H (low-pass) and G (high-pass), respectively. The wavelet packet subspace with modulation frequency index n and bandwidth index j is then defined as

$$\begin{aligned}U_j^n = \mathrm{Clos}_{L^2(\Re)}\{\varphi_{j,k}^n(x) = 2^{-j/2}\psi_n(2^{-j}x-k):\ k\in Z\}\\ j\in Z, n\in Z_+.\end{aligned} \tag{9}$$

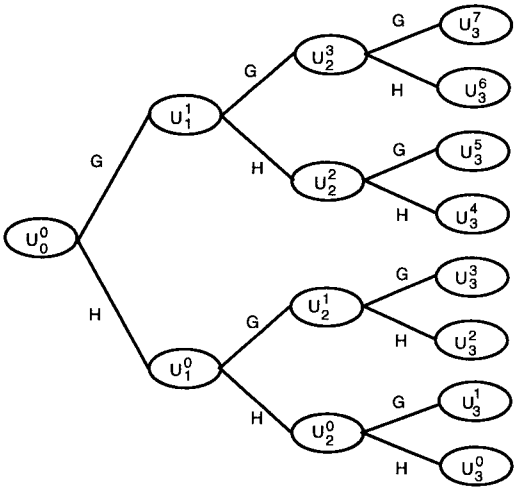

Fig. 1. Wavelet packet decomposition tree.

The wavelet packet space can be decomposed into two subspaces

$$U_j^n = U_{j+1}^{2n} \oplus U_{j+1}^{2n+1}, \qquad j\in Z. \tag{10}$$

From the scaling function space V and the wavelet function space W in multiresolution analysis, we define the initial wavelet packet spaces as $U_0^0 = V$ and $U_0^1 = W$. Therefore, the signal space S can be decomposed into the following wavelet packet subspaces:

$$\begin{aligned}S &= U_0^0 \oplus U_0^1\\ &= U_1^0 \oplus U_1^1 \oplus U_1^2 \oplus U_1^3\\ &= U_2^0 \oplus U_2^1 \oplus U_2^2 \oplus U_2^3 \oplus U_2^4 \oplus U_2^5 \oplus U_2^6 \oplus U_2^7\\ &\cdots\\ &= U_k^0 \oplus U_k^1 \oplus U_k^2 \oplus \cdots \oplus U_k^{2^{k+1}-1}.\end{aligned} \tag{11}$$

Note that the wavelet packet space is the further decomposition of both the scaling function space and the wavelet space, and the frequency bands corresponding to V and W are partitioned into 2^k "subbands" in the wavelet packet transform. Fig. 1 shows the wavelet packet decomposition tree. For the wavelet packet basis function $\varphi_{j,k}^n$ in (9), we define its dyadic interval $I_{j,n} \subset \Re$ in the frequency domain as [11]

$$I_{j,n} = [2^{-j}n, 2^{-j}(n+1)). \tag{12}$$

If the basis $\{\varphi_j^n\}$ of the wavelet packet transform is chosen from the decomposition tree, their dyadic intervals should be disjoint and cover the entire signal bandwidth, i.e.,

$$\bigcap_{j,n} I_{j,n} = [\emptyset]. \tag{13}$$

and

$$\bigcup_{j,n} I_{j,n} = [0,1). \tag{14}$$

Therefore, the wavelet packet basis $\{\varphi_j^n\}$ is a modulated wavelet with a center frequency of $2^{-j}(n+1/2)$ and a bandwidth of 2^{-j}, which are normalized with respect to the bandwidth of the input signal. At different stages of the decomposition tree, the projections of the original data

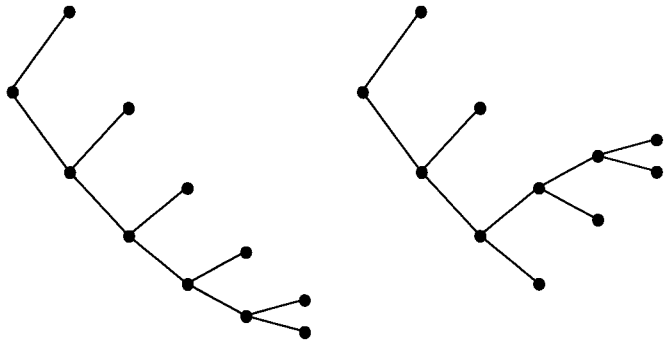

(a) (b)

Fig. 2. The decomposition tree structure of (a) the conventional wavelet transform (CWT) and (b) the adaptive wavelet packet transform (AWPT).

onto the wavelet packet basis spaces have different spatial and spectral resolution. The original input data sequence discretized in the space domain has the best spatial resolution, but the worst spectral resolution. If the signal is decomposed with the wavelet packet basis, as we go deeper into the decomposition tree from the top stage to the bottom stage, the decomposed data have better spectral resolution but worse spatial resolution. The full wavelet packet decomposition is equivalent to an FFT with the basic wavelet as the filter bank function. The wavelet packet decomposition at any stage between the top stage and the bottom stage in the decomposition tree is equivalent to a short-time Fourier transform (STFT) with different space windows. Finally, as shown in Fig. 2(a), the conventional wavelet basis is a wavelet packet basis that consistently decomposes along the lower frequency band until it reaches the bottom stage. Thus the FFT, STFT, and CWT can all be considered as special cases of the wavelet packet transform with a prescribed tree structure. In general, a wavelet packet basis consists of functions with different scales, corresponding to the different depths along the decomposition tree, as shown in Fig. 2(b). Yet they should satisfy the orthogonality and completeness requirements in (13) and (14). Of all the eligible wavelet packet bases (which include the CWT, FFT, and STFT bases), not all of them are good for accomplishing the goal of moment matrix sparsification. We shall search and find such a wavelet packet basis from all possible cases to create the maximum sparsity in the resulting transformed matrix.

B. Implementation of Moment Matrix Transform with Wavelet Packet Basis

The transformation of the moment matrix from a standard pulse basis to a general wavelet packet basis can be implemented via a two-channel filter bank structure. Let us consider a discretized data sequence in the space domain $\{s(n)\}$ to be transformed from a standard basis to a wavelet packet basis. The original sequence can be considered approximately as the projection of the original analog signal onto the signal space constructed from the wavelet packet basis with the highest spatial resolution

$$s(n) = \int s(x)\phi(x-n)\,dx = \langle s(x), \varphi^0_{0,n}(x)\rangle \tag{15}$$

where $\phi(\boldsymbol{x})$ is the scaling function corresponding to the wavelets chosen for the application, and φ is the wavelet packet basis defined in (9). Since the wavelet packet basis satisfies the two-scale equations [15], [16], the first stage of the wavelet packet decomposition tree is

$$\begin{aligned} s^1_0(n) &= \langle s(x), \varphi^0_{1,n}(x)\rangle \\ &= \left\langle \sum_k s(k)\varphi^0_{0,k}(x), \varphi^0_{1,n}(x)\right\rangle \\ &= \sum_k s(k)h(2n-k). \end{aligned} \tag{16}$$

Similarly

$$s^1_1(n) = \sum_k s(k)g(2n-k). \tag{17}$$

The sequences $s^1_0(n)$ and $s^1_1(n)$ are then decomposed further in the second stage of the wavelet packet decomposition tree

$$\begin{aligned} s^2_{00}(n) &= \sum_k h(2n-k)s^1_0(k) \\ s^2_{01}(n) &= \sum_k g(2n-k)s^1_0(k) \\ s^2_{10}(n) &= \sum_k h(2n-k)s^1_1(k) \\ s^2_{11}(n) &= \sum_k g(2n-k)s^1_1(k). \end{aligned} \tag{18}$$

Following the same procedure, the outputs of the full wavelet packet decomposition are

$$\begin{aligned} &\{s(n)\} \\ &\{s^1_0(n), s^1_1(n)\} \\ &\{s^2_{00}(n), s^2_{01}(n), s^2_{10}(n), s^2_{11}(n)\} \\ &\{s^3_{000}(n), s^3_{001}(n), s^3_{010}(n), s^3_{011}(n), s^3_{100}(n), s^3_{101}(n) \\ &\quad s^3_{110}(n), s^3_{111}(n)\} \\ &\cdots. \end{aligned} \tag{19}$$

The decompositions from the sequence $s^i_n(n)$ at stage i into the sequences $s^{i+1}_{m0}(n)$ and $s^{i+1}_{m1}(n)$ at stage $i+1$ using the two decomposition quadrature filters are given by

$$\begin{aligned} s^{i+1}_{m0}(n) &= \sum_k h(2n-k)s^i_m(k) \\ s^{i+1}_{m1}(n) &= \sum_k g(2n-k)s^i_m(k). \end{aligned} \tag{20}$$

This decomposition is equivalent to first passing the input sequence through the two decomposition quadrature filters and then down-sampling the outputs by two (discarding every other data sample). Conversely, the sequence $s^i_m(n)$ at stage i can be perfectly reconstructed from the two sequences $s^{i+1}_{m0}(n)$ and $s^{i+1}_{m1}(n)$ at stage $i+1$ using two reconstruction quadrature filters, P and Q.

$$s^i_m(n) = \sum_k p(n-2k)s^{i+1}_{m0}(k) + \sum_k q(n-2k)s^{i+1}_{m1}(k) \tag{21}$$

where $\{p(k)\}$ and $\{q(k)\}$ are the impulse responses of P and Q, respectively. For orthogonal wavelet basis, the reconstruction filters P and Q and the decomposition filters H and G are exactly the same except that their impulse responses are the space-reversed versions of each other. The reconstruction is equivalent to first up-sampling the two sequences by two (inserting a zero between two data samples), passing the resulting sequences through the two reconstruction quadrature filters, and then summing the two outputs.

From the above discussion, we can now implement the transformations of the moment equation in (2)–(7) efficiently with repeated two-channel filtering and down (or up)-sampling rather than direct matrix multiplication. If a vector is right multiplied with the transformation matrix, it can be realized with the repeated filtering and down-sampling of the vector with filters H and G in (20). If a vector is left multiplied with the transformation matrix, it can be realized with the repeated up-sampling and filtering (reconstruction) of the vector with filters P and Q in (21).

To implement the moment equation transformations, we first rewrite (4) and (6) into the following forms:

$$[\tilde{\boldsymbol{Z}}] = [\boldsymbol{M}_2]^T[\boldsymbol{Z}][\boldsymbol{M}_1] = \{\{[\boldsymbol{Z}][\boldsymbol{M}_1]\}^T[\boldsymbol{M}_2]\}^T \quad (22)$$

$$[\tilde{\boldsymbol{E}}] = [\boldsymbol{M}_2]^T\boldsymbol{E} = \{\boldsymbol{E}^T[\boldsymbol{M}_2]\}^T. \quad (23)$$

In this manner, all the rows of the original moment matrix are first decomposed from their original basis functions to the wavelet packet basis, and then all the columns are decomposed from the original testing functions to the wavelet packet testing basis. Similarly the original excitation vector is decomposed to be represented with the wavelet packet testing basis. All the decomposition can be implemented by filtering and down-sampling with filters H and G. Finally, to reconstruct the original induced current vector $\boldsymbol{J}$ once the transformed induced current $\tilde{\boldsymbol{J}}$ is found, we implement (7) via up-sampling and filtering with filters P and Q.

C. Best Wavelet Packet Basis Search for AWPT Moment Matrix Transform

To search for the best wavelet packet bases to achieve the maximum sparsity in the transformed moment matrix, a cost function is defined to evaluate the sparsity of the transformed matrix for a specific basis. The sparser the transformed moment matrix, the smaller the value of the cost function should be. A commonly used cost function is the additive energy concentration function defined as [11], [12]

$$C(\boldsymbol{Z}) = \sum_m \sum_n |Z(m,n)|^p, \qquad p < 2. \quad (24)$$

In our application we choose $P = 1$ and use the approximation $|Z| \approx |\mathrm{Re}(Z)| + |\mathrm{Im}(Z)|$ to speed up the computation time of the cost function

$$C(\boldsymbol{Z}) = \sum_m \sum_n (|\mathrm{Re}(Z(m,n)| + |\mathrm{Im}(Z(m,n)|). \quad (25)$$

When the rows and columns of the moment matrix are being decomposed from the top stage to the bottom stage in the decomposition tree, the cost function is calculated at every stage to evaluate the sparsity of the transformed matrix. It is then compared against that of the next stage to decide whether the matrix should be further decomposed. If the total cost of the decomposed matrix is reduced, the decomposition is accepted and further decomposition is applied. Otherwise the decomposed matrix is rejected and the decomposition stops. The maximum number of decomposition stages is $\lfloor \log_2(N) \rfloor$. When the decomposition in the wavelet packet decomposition tree stops at some nodes according to the algorithm mentioned above, these nodes consist of the best wavelet packet basis, based on which the transformed moment matrix has the least cost. Obviously the transformation to the best basis is finished when the best basis is found. The same algorithm is applied to the columns of moment matrix to implement the best testing basis search and transformation.

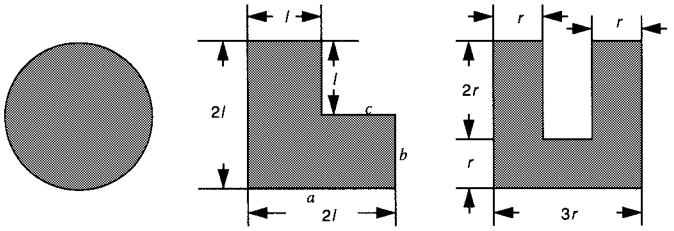

Fig. 3. The geometry of the three test scatterers (a) a circular cylinder; (b) an L-shaped structure; and (c) a duct.

III. Numerical Results

The performance of the AWPT in the sparsification of the moment matrix is tested using several two-dimensional conducting structures. The scatterers considered include a circular cylinder, an L-shaped structure and a duct (Fig. 3). The first two structures are taken from [5]. To avoid the internal resonance problem, the combined-field integral equation (CFIE) is employed to generate the moment matrices with pulse bases $(\Delta = 0.1\lambda)$ and point matching under E-polarized incidence. By changing the physical size of the scatterers proportionally, we obtain moment matrices with sizes ranging from $N = 128$ to 4096. Both the CWT and the AWPT are applied to the sparsification of the matrices. To sparsify the transformed matrices, the elements of the matrices are thresheld with a level that is based on a matrix norm criterion as follows:

$$T = \alpha \cdot \mathrm{Norm}(\boldsymbol{Z})/N = \alpha \cdot \max_m \sum_n |Z(n,m)|/N. \quad (26)$$

The advantage of choosing the threshold level based on the matrix norm is that the relative error of the solution caused by the thresholding is under a predicable limit [18]. Our experiments show that when α is between 1/5 and 1/10, the calculated induced current has a rms error of around 2%. Daubechies filters with the order of 16 (i.e., seven vanishing moments) are used as the quadrature filters through all transformations [19]. Similar results are obtained with other well-defined orthogonal filters such as the Battle–Lemarie filter.

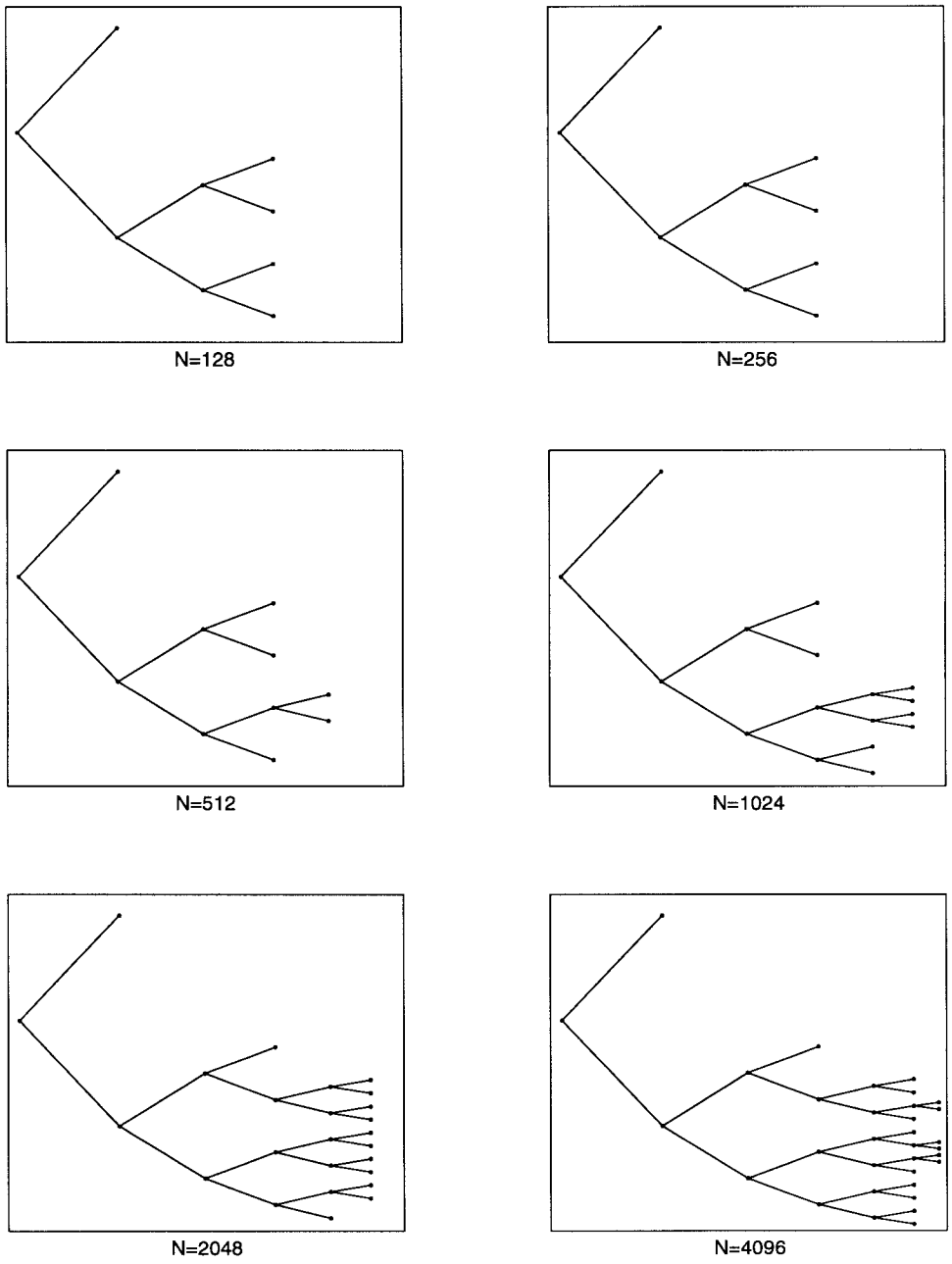

Fig. 4. The AWPT frequency decomposition trees for the duct of various sizes.

The AWPT algorithm described above is applied to the moment matrices from the three scatterers of varying sizes. We find in our examples that the best wavelet packet transform trees after running the algorithm are the same for the expansion basis and the testing basis. This is due to the symmetrical nature of the original moment matrix. Fig. 4 shows the resulting optimal spectral decomposition trees for the duct. It is most interesting to observe that in the best AWPT tree after the adaptive selection procedure, the branch that zooms in the deepest is right around the spectral frequency k_0. (Since the spatial discretization used is $\lambda/10$, the maximum spectral content of the matrix is $10k_0$, which corresponds to a normalized frequency of 2π. k_0, therefore, is equivalent to a normalized frequency of $\pi/5$. The frequency decomposition trees in Fig. 4 display the normalized frequencies from zero to π, and thus the frequency k_0 corresponds to the branch that is about 1/5 of the way from the lowest branch of the tree.) This means that the wavelet packet basis with the largest spatial extent has a spectral content around k0. Therefore, the AWPT tree has automatically adapted itself to this well-known spatial-spectral characteristic of the electrodynamic kernel [7]. Shown in Fig. 5 are the APWT trees for the circular cylinder and the L-shaped structure with $N = 4096$. We observe that the overall structures of the AWPT trees are quite similar for different scatterer shapes. That suggests that the best APWT basis may not be very sensitive to the physical shape of the scatterer.

The transformed moment matrices using the CWT and the AWPT with $N = 512$ for the duct are shown in Fig. 6 with a threshold level parameter of 0.1. It is clearly seen

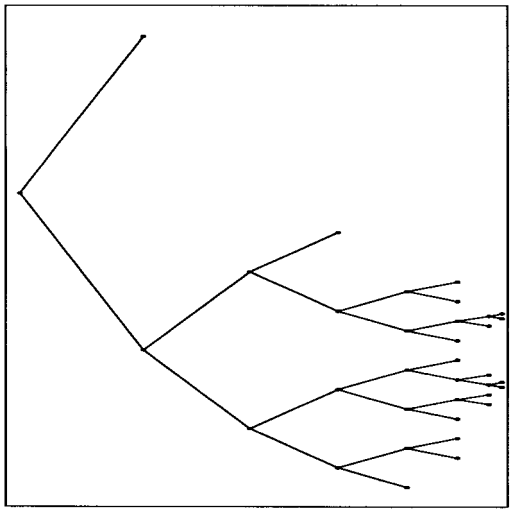

(a)

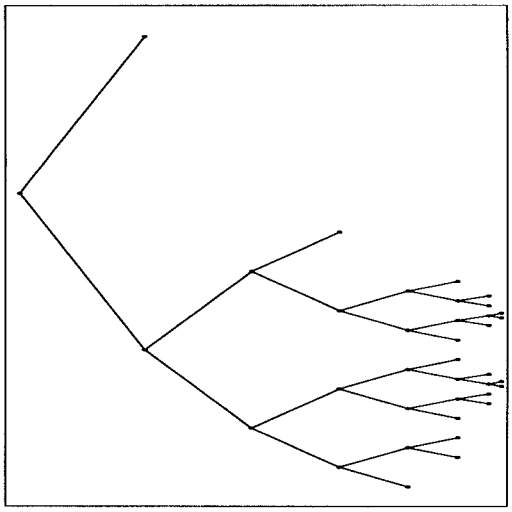

(b)

Fig. 5. The AWPT decomposition trees for (a) the circular cylinder and (b) the L-shaped structure with $N = 4096$.

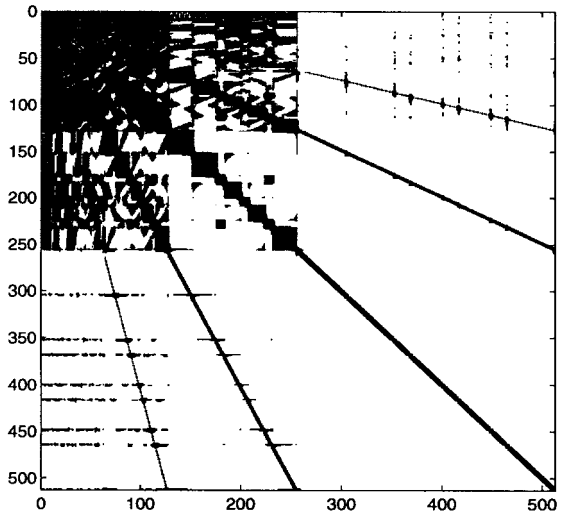

(a)

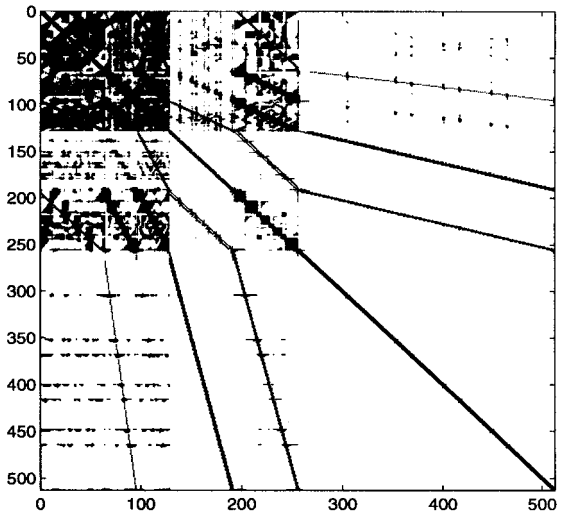

(b)

Fig. 6. The transformed moment matrices for the duct with $N = 512$ using (a) the CWT and (b) AWPT.

that with the AWPT basis the interactions in the upper left corner area of the matrix are reduced. This region corresponds to the interaction of the wavelet functions with the largest spatial extent. As a consequence, the AWPT moment matrices are sparser that the CWT ones. The numbers of nonzero elements in the transformed matrices after thresholding are plotted as a function of problem size for the duct in Fig. 7. It illustrates how the sparsity of the matrices scales according to the problem size. Although not shown, similar results were also obtained for the circular cylinder and the L-shaped structure. For the CWT, the number of nonzero elements grows as $O(N^{1.8})$ for the L-shaped structure and the duct, and as $O(N^{1.9})$ for the circular cylinder, showing only a small reduction from the original $O(N^2)$. The nonzero elements in the AWPT matrices, on the other hand, are found to grow as $O(N^{1.4})$. This is comparable to the theoretical limit of $O(N^{4/3})$ obtainable by the multilevel fast multipole method [20]. Actually when the problem size is small $(N < 1024)$,

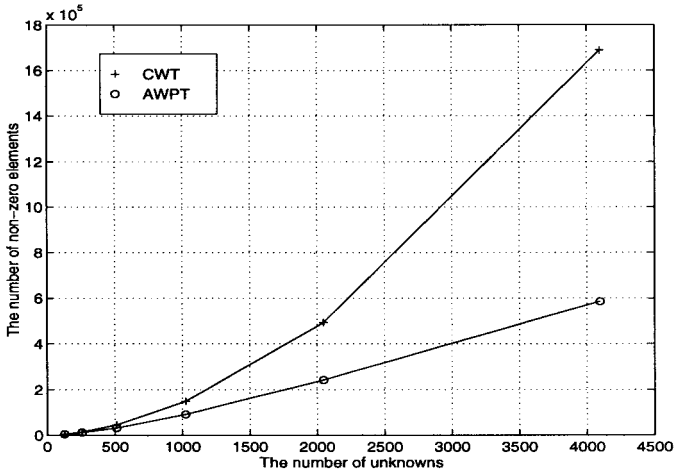

Fig. 7. The number of nonzero elements in the transformed moment matrix after thresholding as a function of problem size N using the CWT and the AWPT for the duct.

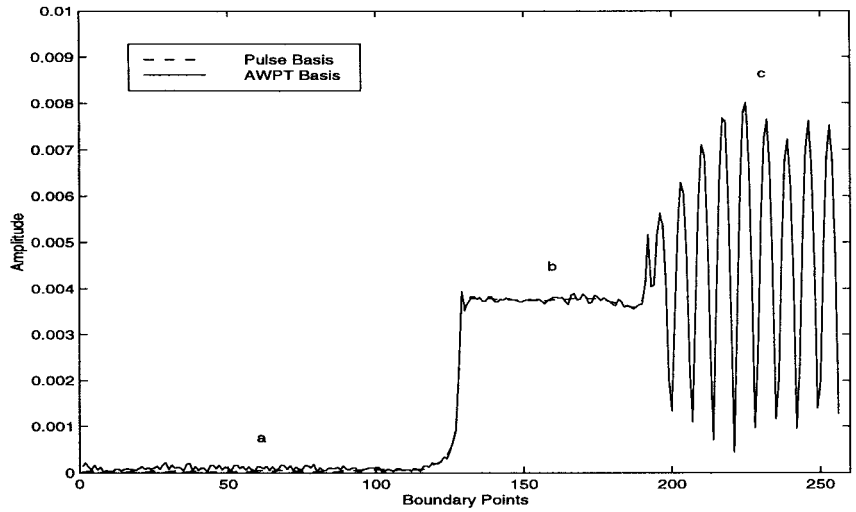

(a)

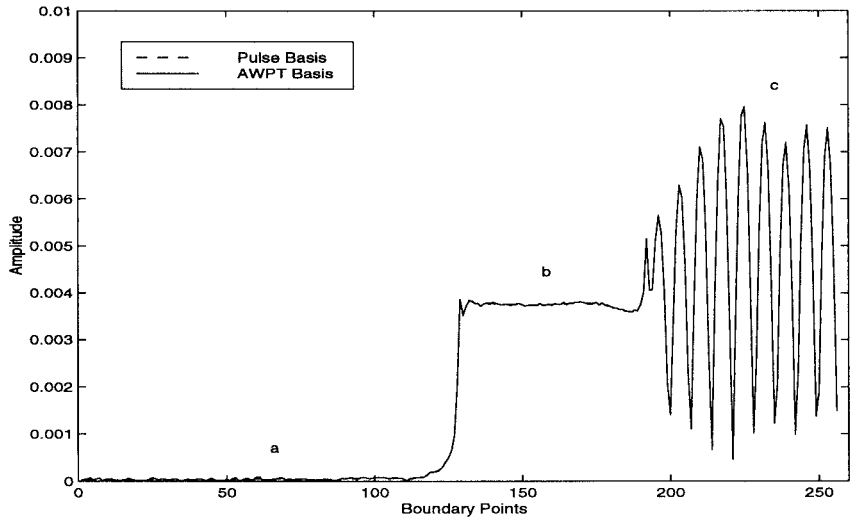

(b)

Fig. 8. The induced current distribution on the L-shaped scatterer with $N = 512$ using AWPT algorithm with the threshold parameter (a) $\alpha = 1/10$ and (a) $\alpha = 1/20$. Also plotted is the reference solution obtained by solving the original dense moment equation. The excitation is incident from an angle of 45° degrees with respect to the c-face of the scatterer.

there is not much difference between the sparsity of the CWT matrices and that of the AWPT matrices. However, when the problem size is increased, the number of the nonzero elements in the thresheld matrix is close to $O(N^2)$ for the CWT, and approaches $O(N^{1.3})$ for AWPT. Therefore, the reduced computation complexity in the AWPT clearly becomes an important advantage for solving large-scale electromagnetic scattering problems. We have also investigated whether the sparsity found above is affected by the threshold level. For the three scatterers considered, we find that when the threshold level parameter α in (26) is changed between 1/5 and 1/40, the sparsity curve is shifted up slightly with a smaller α. However, the nonzero elements in the AWPT matrices still grow at a rate around $O(N^{1.4})$.

Fig. 8(a) shows the induced current distribution of the L-shaped scatterer solved using the AWPT basis from the thresheld matrix with 512 unknowns and a threshold level α of 1/10. The current solved from the original dense moment matrix with pulse basis and point matching is also displayed in the same figure for reference. The rms error for the current solution using the AWPT basis is found to be 1.98% when compared to the reference solution. Fig. 8(b) shows the resulting current solution when the threshold level α is 1/20. The rms error is found to be 0.99%. The results prove that the solutions using the AWPT algorithm are in good agreement with the reference solution when an appropriate threshold level is chosen.

Next, we consider the computation cost for carrying out the AWPT procedure. For a problem with size of N, the maximum number of AWPT decomposition stages is $\log_2(N)$. Theoretically the computation complexity for a full decomposition of a moment matrix using APWT is $O(N^2 \log_2(N))$. The additional computation cost for the evaluation of the cost function is bounded by $O(N^2)$ addition operations. However, as we have observed, the AWPT decomposition of the moment matrix tends to zoom in only along the frequency k_0. The

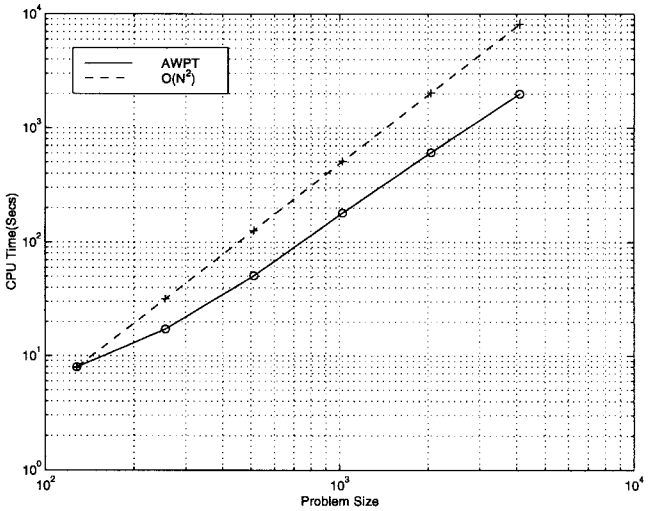

Fig. 9. CPU run time required to implement the AWPT algorithm as a function of problem size N. The moment matrices of L-shaped scatterer are used for the experiment.

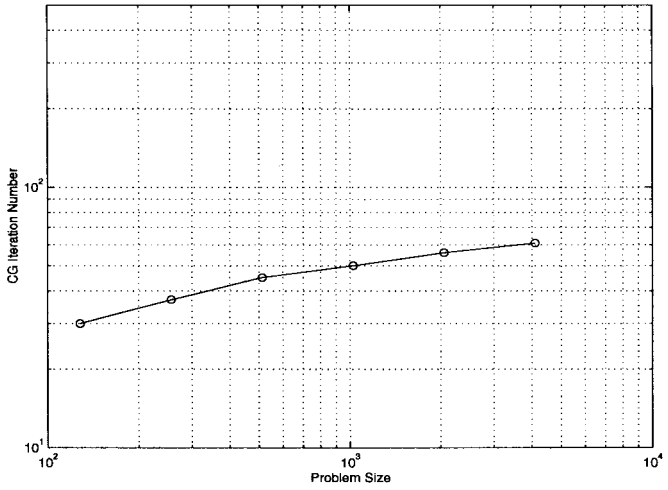

Fig. 10. The iteration number of solving the AWPT basis moment equations using the conjugate gradient (CG) method as a function of problem size N.

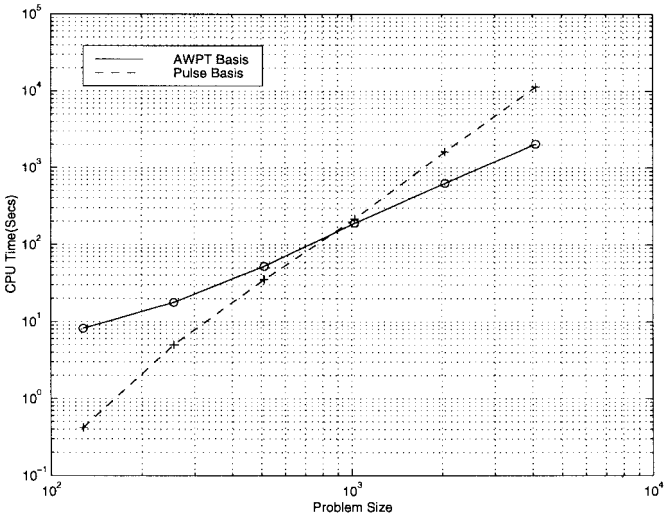

Fig. 11. The total CPU run time required to solve the moment equations using the AWPT together with the CG algorithm versus that of solving the original moment equations using the CG method only, plotted as a function of problem size N.

actually observed operations needed to implement the AWPT is much less than the estimated limit. Fig. 9 shows the actual CPU run time to implement the AWPT as a function of problem size. The theoretical upper bound of $O(N^2)$ based on the first data point is shown as the dotted line in the same figure. It is observed that the actual CPU run time for the AWPT procedure is less than $O(N^2)$.

Finally, we apply the conjugate gradient (CG) algorithm to solve the AWPT matrix equation [21]. The complexity of the CG solver depends on the iteration number in addition to the complexity of the matrix-vector multiplication. The iteration number is directly related to the condition number of the matrix. Fig. 10 shows the iteration number of the AWPT sparsified system in a CG solver as a function of problem size for the L-shaped scatterer. The CG convergence criterion is based on the relative residual, i.e.,

$$\text{Norm}\,(\tilde{\boldsymbol{E}} - \tilde{\boldsymbol{Z}}\hat{\tilde{\boldsymbol{J}}})/\text{Norm}\,(\tilde{\boldsymbol{E}}) < 10^{-8}. \tag{27}$$

It can be seen that there is only a slight increase in the iteration number in the CG solver as the problem size grows. Consequently, the total complexity of solving the AWPT moment equation is mainly determined by the complexity of the matrix-vector multiplication, i.e., the number of nonzero elements in the matrix. Therefore, the complexity for computing the induced current on a scatterer using the AWPT is around $O(N^{1.4})$ operations with an additional upper-bound of $O(N^2)$ operations for the transformation from the original basis to the AWPT basis. Note that although the cost for implementing the AWPT algorithm is around $O(N^2)$, this is only a one-time overhead. When solving multiple right-hand-side problems, this cost is incurred only once while the reduced $O(N^{1.4})$ cost of solving the transformed equations is repeated for each right-hand side. This should be compared to the direct solution of the dense moment matrix using the CG method which requires $O(P \cdot N^2)$ operations for each right-hand side. Fig. 11 shows the total CPU run time required to solve the moment equations for the L-shaped scatterer with a single right-hand side using the AWPT method, which includes both the transformation time and the CG solution time. It is compared against the time required to solve the original dense matrix equation using the CG algorithm only. It can be seen that when the problem size N is sufficiently large, the time required to solve the electromagnetic integral equation is greatly reduced by using the AWPT method.

IV. Conclusions

The adaptive wavelet packet transform is applied to the sparsification of moment matrices for the fast solution of electromagnetic integral equations. The AWPT algorithm can adaptively track the oscillatory frequency of the Green's function and generate an efficient decomposition of the original moment matrix. It is found that the sparsified moment matrix after thresholding has only $O(N^{1.4})$ significant elements for typical scatterers. Accordingly the complexity to solve the transformed moment equation using the conjugate gradient

method is around $O(N^{1.4})$ operations. Although there is an additional upper bound cost of $O(N^2)$ required to implement the AWPT algorithm, the overall complexity to solve electromagnetic integral equations is significantly reduced.

In the AWPT algorithm described, the best basis is searched in a progressive fashion from the root to the branches in the wavelet packet tree. The basis found in this manner is only a local optimum basis. The global best basis can be found using a pruning algorithm proposed in [22]. However, such algorithm would require significantly more computation time and memory.

The cost function in our AWPT algorithm is the energy concentration function with power of one rather than the popular entropy-based cost function. We have chosen this intentionally to avoid the multiplication operation in the evaluation of the cost function, and make its complexity negligible compared with that of the AWPT itself.

A key drawback of the present algorithm is that the total CPU run time for the solution of electromagnetic equations must include the AWPT implementation time. In addition, the approach still requires the original moment matrix be generated and stored prior to the AWPT procedure. Therefore there exists an $O(N^2)$ memory bottleneck in this procedure. A way to overcome both the time and memory bottleneck is to fill the moment matrix elements using the AWPT basis directly. Future work should be devoted to finding an efficient way to estimate the best AWPT basis, and to achieve the transform with less computation.

Finally, the application of the AWPT to the moment matrix basis transformation is implemented in this paper as a separable tensor product of two one-dimensional (1-D) wavelet packet transforms, which are separately applied to all rows and all columns of the matrix. This kind of transformation is easier to implement and interpret with basis transformation concept than the 2-D quadtree decomposition methodology often used in image compression. However, we have found from our preliminary tests that the latter approach can potentially sparsify moment matrix to only $O(N)$ significant elements. Unfortunately, this sparsity is difficult to be utilized because there is no efficient way to project the excitation vector and the induced current vector to the 2-D quadtree basis.

ACKNOWLEDGMENT

The authors thank Profs. W. Chew and W. Golik for helpful comments on the manuscript.

REFERENCES

[1] B. Z. Steinberg and Y. Leviatan, "On the use of wavelet expansions in the method of moments," *IEEE Trans. Antennas Propagat.*, vol. 41, pp. 610–619, May 1993.
[2] H. Kim and H. Ling, " On the application of fast wavelet transform to the integral equations solution of electromagnetic scattering problems," *Microwave Opt. Technol. Lett.*, vol. 6, pp. 168–173, Mar. 1993.
[3] K. Sabetfakhri and L. P. B. Katehi, "Analysis of integrated millimeter-wave and submillimeter-wave waveguides using orthonormal wavelet expansion," *IEEE Trans. Microwave Theory Tech.*, vol. 42, pp. 2412–2422, Dec. 1994.
[4] G. Wang and G. Pan, "Full wave analysis of microstrip floating line structures by wavelet expansion method," *IEEE Trans. Microwave Theory Tech.*, vol. 43, pp. 131–142, Jan. 1995.
[5] R. L. Wagner and W. C. Chew, "A study of wavelets for the solution of electromagnetic integral equations," *IEEE Trans. Antennas Propagat.*, vol. 43, pp. 802–810, Aug. 1995.
[6] Z. Baharav and Y. Leviatan, "Impedance matrix compression using adaptively constructed basis functions," *IEEE Trans. Antennas Propagat.*, vol. 44, pp. 1231–1238, Sept. 1996.
[7] H. Kim, H. Ling, and C. Lee, "A fast moment method algorithm using spectral domain wavelet concepts," *Radio Sci.*, vol. 31, pp. 1253–1261, Sept.–Oct. 1996.
[8] H. Deng and H. Ling, "Moment matrix sparsification using adaptive wavelet packet transform," *Electron. Lett.*, vol. 33, pp. 1127–1128, June 1997.
[9] G. Beylkin, R. Coifman, and V. Rokhlin, "Fast wavelet transforms and numerical algorithms I," *Com. Pure Appl. Math.*, vol. 44, pp. 141–183, 1991.
[10] R. R. Coifman, Y. Meyer, and M. V. Wickerhauser, "Size properties of wavelet packets," in *Wavelets and Their Applications*. Boston, MA: Jones and Bartlett, 1992.
[11] M. V. Wickerhauser, *Adapted Wavelet Analysis from Theory to Software*. Wellesley, MA: A. K. Peters, 1994.
[12] C. Tasell, "Top-down and bottom-up tree search algorithms for selecting bases in wavelet packets transforms," in *Proc. Vilard de Lans Conf.* Berlin, Germany: Springer-Verlag, 1995.
[13] W. L. Golik and D. S. Wang, "Fast wavelet packet algorithm for the combined field integral equation," in *Proc. 13th Annu. Rev. Progress in Applied Computational Electromagnetics*, Monterey, CA, Mar. 1997.
[14] W. L. Golik, "Wavelet packets for fast solution of electromagnetic integral equations," *IEEE Trans. Antennas Propagat.*, vol. 46, pp. 618–624, May 1998.
[15] C. K. Chui, *An Introduction to Wavelets*. New York: Academic, 1992.
[16] L. R. Montefusco, "Parallel numerical algorithms with orthonormal wavelet packet bases," *Wavelets: Theory, Algorithms, and Application.* New York: Academic, 1994.
[17] M. Wang, A. K. Chan, and C. K. Chui, "Linear frequency modulated signal detection using wavelet packets, ambiguity function and Radon transform," in *Proc. 1995 IEEE Antennas Propagat. Soc. Int. Symp.*, CA, June 1995, pp. 308–311.
[18] B. Alpert, G. Beylkin, R. Coifman, and V. Rokhlin, "Wavelet-like bases for the fast solution of second-kind integral equations," *SIAM J. Sci. Comp.*, vol. 14, pp. 159–184, Jan. 1993.
[19] I. Daubechies, "Orthonormal bases of compactly supported wavelets," *Comm. Pure Appl. Math.*, vol. 41, pp. 909–996, 1988.
[20] R. L. Wagner and W. C. Chew, "A ray-propagation fast multipole algorithm," *Microwave Opt. Technol. Lett.*, vol. 7, pp. 435–438, July 1994.
[21] J. C. Gilbert and J. Nocedal, "Global convergence properties of conjugate gradient methods for optimization," *SIAM J. Optimization*, vol. 2, pp. 21–42, 1992.
[22] R. R. Coifman and M. V. Wickerhauser, "Entropy-based algorithms for best basis selection," *IEEE Trans. Inform. Theory*, vol. 38, pp. 713–718, Mar. 1992.

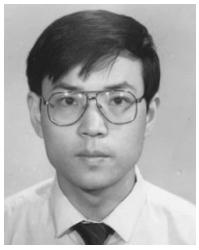

Hai Deng (S'97) was born in Tongcheng, Anhui, China, in 1967. He received the B.S.E.E. degree from Anhui University in 1987 and the M.S.E.E. degree from Beijing Institute of Technology in 1990. He has been a Ph.D. student and a research assistant in the Electrical and Computer Department at the University of Texas at Austin since 1996.

From 1990 to 1996, he was a Design Engineer, and later a Senior Engineer at Beijing Institute of Radio Measurement, Beijing, China. His research interests include radar signal processing, wavelet applications to computational electromagnetics, target identification, wireless communications, and logic and VLSI design.

Hao Ling (S'83–M'86–SM'92–F'99), for a photograph and biography, see p. 1453 of the November 1996 issue of this TRANSACTIONS.